Cumhuriyet Science Journal

Cumhuriyet Sci. J., 46(1) (2025) 152-161
DOI: https://doi.org/10.17776/csj.1589607

| csj.cumhuriyet.edu.tr | Founded: 2002 ISSN: 2587-2680 e-ISSN: 2587-246X Publisher: Sivas Cumhuriyet University

Electronic, Optical and Mechanical Properties of Ta Doped LiNbO3: Ab Initio Calculation

Furkahan Acar [1,a] Şevket Şimşek [2,b,*]

[1] *Department of Material Science and Engineering, Faculty of Engineering, Hakkari University, 30000, Hakkari, Türkiye*[3]
**Corresponding author*

Research Article

History
Received: 22/11/2024
Accepted: 31/01/2025

ABSTRACT

In this study, the electronic, optical and mechanical properties of $LiNb_{1-x}Ta_xO_3$ were investigated by ab initio method by adding tantalum (Ta) instead of niobium (Nb) with 0.1 doping step from x=0 to x=1 at different concentrations. The effects of Ta addition on the electronic structure of $LiNbO_3$ were investigated. The results indicate that Ta doping results in an increase in the forbidden band gap of $LiNbO_3$. The real and imaginary parts of the dielectric function of $LiNb_{1-x}Ta_xO_3$ were calculated and the optical transitions between the bands were determined. The second-order elastic constants of Ta doped $LiNbO_3$ were calculated and the mechanical stability of the material was determined. In addition, the calculated elastic constants were used to determine the bulk modulus (B), shear modulus (G), Young's modulus (E), H_{macro} and H_{micro} hardness values. It was determined that the $LiNb_{1-x}Ta_xO_3$ material exhibited a transition from a ductile to a more brittle state with the addition of Ta.

Keywords: $LiNbO_3$, $LiTaO_3$, Electronic properties, Optical properties, Elastic properties.

[a] acarfurkahan@gmail.com https://orcid.org/0000-0002-4750-5036 [b] ssimsek@hakkari.edu.tr https://orcid.org/0000-0002-7260-6437

Introduction

$LiNbO_3$ (Lithium niobate), a member of the ABO_3-type ferroelectric perovskite family, is one of the most technologically important materials for optoelectronics. Its versatility stems from its considerable piezoelectric coefficient and distinctive electro-optical, acoustic-optical, nonlinear optical, photorefractive and photoconductive characteristics. It is employed in a multitude of applications, including waveguides, solid-state lasers, photorefractive devices and other optoelectronic devices. The LN (Lithium Niobate) crystal has been designated as "Optical Silicon"[1]. The properties of LN crystals can be modified or controlled by the introduction of specific dopants. As an example, the photorefractive (PR) properties of LN crystals can be significantly suppressed when doped with optically damage-resistant (ODR) ions, such as Sc^{3+}, In^{3+}, Zn^{2+}, and Mg^{2+}, at relatively high concentrations. This allows the frequency to double [2]. Furthermore, doping LN with transition metal ions, including Cu, Fe, Mn, and Ce, can result in the formation of crystals with notable photorefractive properties, rendering them as prospective materials for holographic memory applications [3, 4]. It is known that perovskite oxides, characterized by the general formula ABO_3, display a diverse array of physical properties, including a superconductivity, substantial magnetoresistance, ferroelectric polarization, and high dielectric constant. As a result, it constitutes one of the most crucial categories of materials for technological applications. LN exhibits a paraelectric phase with a trigonal crystal structure, with the R-3c space group, at high temperatures. When subjected to low temperatures, the material undergoes a transformation into a ferroelectric phase characterized by R3c symmetry. A slight deformation of the paraelectric phase is observed in what is known as the ferroelectric phase. In the trigonal ferroelectric phase at room temperature, LN is assigned to the 3m point group [5]. It exhibits spontaneous polarization along the [111] crystal direction in the ferroelectric phase, rendering it an appropriate material for use in optoelectronic devices [6, 7].

To the best of our knowledge, there is no study on the effect of Ta doping on the structural, electronic, optical and mechanical properties of $LiNbO_3$ using the virtual crystal approximation (VCA) [8]. The aim of this study is to investigate the effect of Ta doping on the physical properties of LiNbO3 using VCA based on density functional methods (DFT) [9]. For this purpose, the effects of Ta doping on the crystal structure, forbidden band gaps, optical properties such as reflection, refraction, absorption and energy loss function, elastic constants and elastic modulus (such as bulk, shear and Young's modulus) of $LiNbO_3$ with 0.1 doping step from x=0 to x=1 will be investigated.

Materials and Methods

The electronic, optical and elastic properties of Ta-doped $LiNbO_3$ were calculated by means of density functional methods under the generalized gradient approximation (GGA) [9]. The calculations were performed using optimized norm-preserving Vanderbilt

pseudopotentials [10]. The kinetic energy cut-off required for electronic wave functions was determined to be 44 Hartree. In the calculations, the valence electrons of the Li atom were taken to be $1s^2\ 2s^1$, those of the Nb atom $4s^24p^64d^45s^1$, those of the Ta atom $5s^25p^65d^36s^2$, and those of the O atom $2s^22p^4$. In order to calculate the electronic and optical properties at specific k points within the Brillouin zone, the 8x8x8 and 16x16x16 Monkhorst-Pack [11] meshes were employed, respectively. In this study, all results were obtained using the VCA. The structural, electronic, optical, and elastic properties of $LiNb_{1-x}Ta_xO_3$ were investigated by ab initio method, wherein Ta was added in place of Nb with a 0.1 doping step from x=0 to x=1 at varying concentrations. All calculations were conducted using the ABINIT software program [12].

Results and Discussion

Structural Properties

$LiNbO_3$ exists in the ferroelectric phase at room temperature, exhibiting a rhombohedral structure (with space group R3c (#161)). Figure 1(a) illustrates the rhombohedral unit cell of the $LiNbO_3$ crystal in its ferroelectric phase. The $LiNbO_3$ unit cell contains two molecules with ten atoms in the rhombohedral structure. The equilibrium lattice parameter of the $LiNbO_3$ crystal was calculated by minimizing the ratio of the total energy of the crystal to its volume. The resulting lattice parameters are presented in Table 1. The obtained values were compared with the theoretical and experimental lattice parameters that have been previously reported in the literature. As illustrated in Table 1, the lattice constant and the angle between the axes determined in this study using the GGA are slightly bigger than those reported in the literature.

Table 1. The relaxed lattice parameters and angles of $LiNbO_3$ in rhombohedral structure.

Method	$a = b = c$ (Å)	$\alpha = \beta = \gamma$
GGA(Cal.)	5.540	58.9
Exp.[13]	5.494	55.8
Exp.[14]	5.496	55.8
GGA[15]	5.509	55.8
GGA[16]	5.495	55.8
LDA[17]	5.488	54.8

Figure 1(b) depicts the variation of lattice parameters for $LiNb_{1-x}Ta_xO_3$ as a function of Ta doping. As illustrated in Figure 1(b), it is clear that the lattice parameters of $LiNbO_3$ exhibit a decrease with Ta doping.

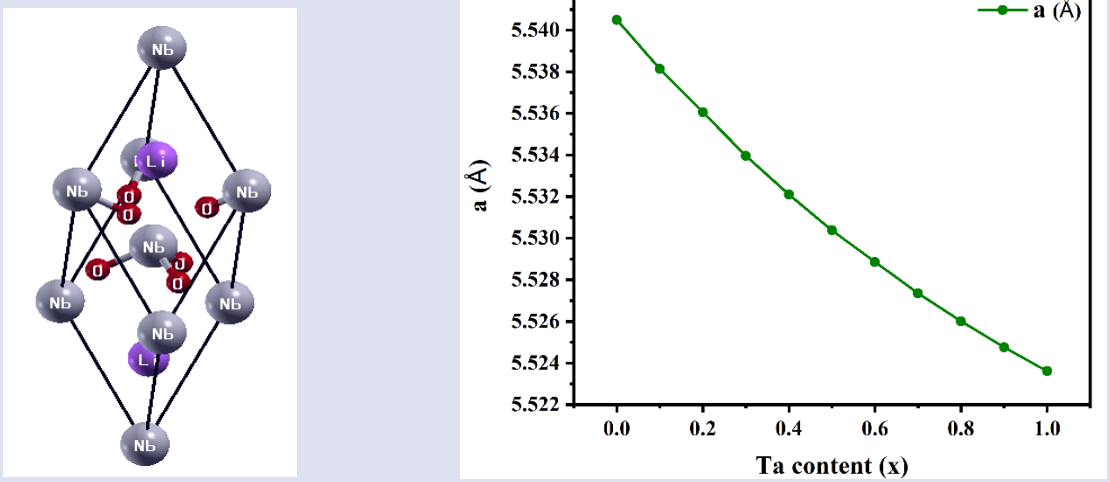

(a) (b)

Figure 1. (a) The rhombohedral unit cell of the LiNbO3 crystal in the ferroelectric phase and (b) the calculated lattice parameter as a function of Ta doping.

Electronic Properties

An understanding of the electronic band structure is crucial for the determination of the electrical properties of materials, including their conductive, semiconductive, and insulating characteristics. This knowledge is also essential for technological applications. The electronic band structure and density of state (DOS) plots of $LiNb_{1-x}Ta_xO_3$ for x=0.0 and x=0.5 are presented in Figure 2(a) and (b), respectively. The Fermi energy level is designated as the zero energy level and is indicated by the red dashed lines. As illustrated in Figure 2(a), the maximum point of the valence band and the minimum point of the conduction band for the $LiNbO_3$ crystal are situated at the Γ point. Consequently, the results of our calculations indicate that the $LiNbO_3$ crystal is a direct bandgap material. In this study, the calculated forbidden energy gap value for $LiNbO_3$ crystal is 3.38 eV. The results obtained in this study and the existing theoretical and

experimental results in the literature are given in Table 2. As illustrated in Table 2, the results obtained are in agreement with the theoretical results available in the literature, but slightly lower than the experimental result obtained by optical measurements. It is known that the forbidden band gaps calculated by DFT are lower than the experimental results obtained by optical measurements because they do not include both quasi-particle effects and excitonic effects [15].

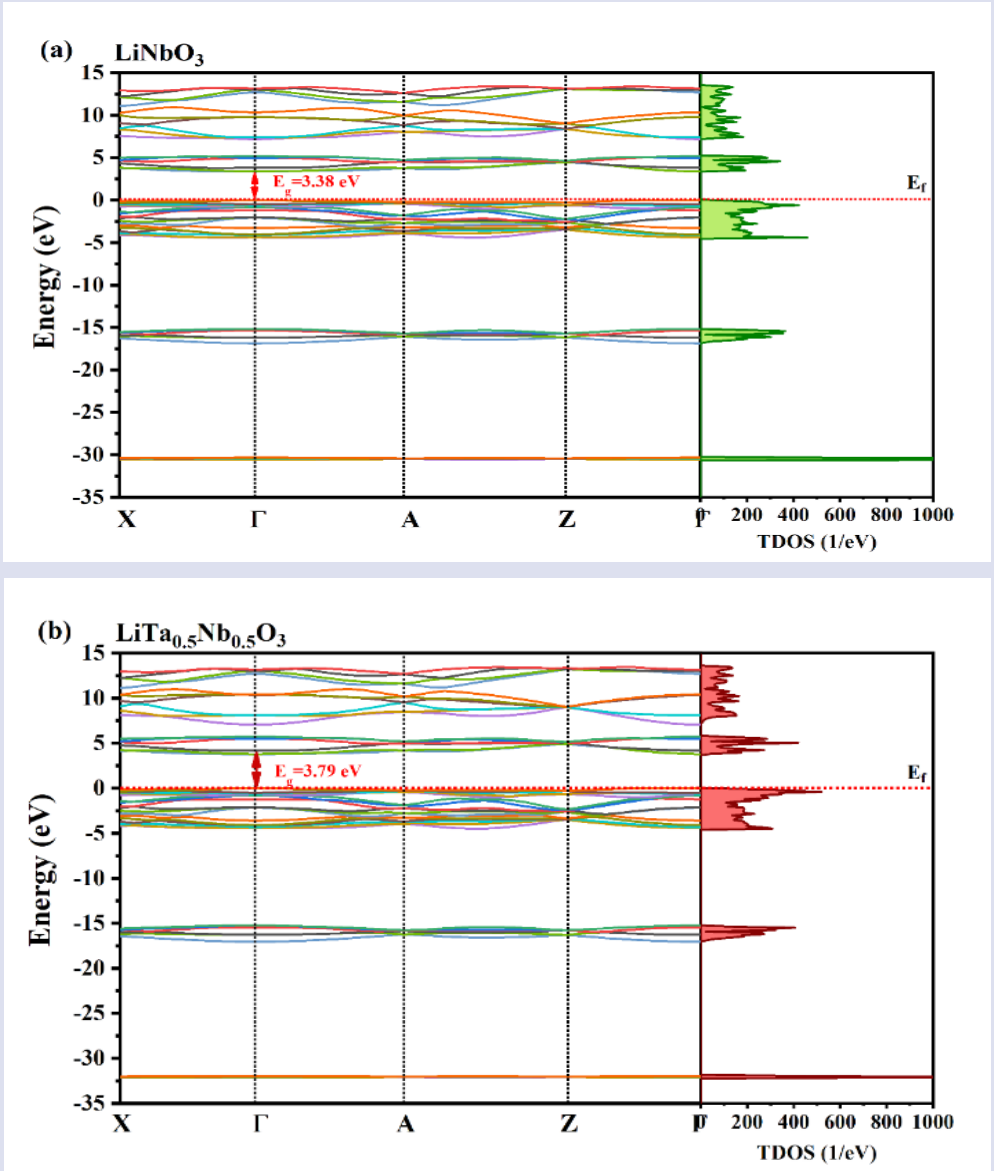

Figure 2. The band structure of $LiNb_{1-x}Ta_xO_3$ for (a) x= 0.0 and (b) x=0.5.

Table 2. Theoretical and experimental band gaps of $LiNbO_3$ and $LiTaO_3$.

Crystal	E_g. LDA (eV)	E_g. GGA (eV)	E_g. Exp. (eV)
$LiNbO_3$	3.40[5]	3.38[Cal.]	3.78[18]
	2.84[19]	3.48[15]	
	3.59[20]	3.61[21]	
	3.35[22]	3.041[19]	
	3.54[17]	3.32[16]	
$LiTaO_3$		4.15[Cal.]	4.70[23]
		3.93[24]	

In order to better understand the nature of the electronic band structure of the $LiNbO_3$ crystal, the partial (PDOS) and total density of states (TDOS) were calculated. As seen in Figure 3(a), the bands between -30 and -32 eV appear to originate from Nb-4p orbitals. The bands between -15 and -17.5 eV are formed by O-2s orbitals. The bands just below the Fermi energy level (between 0 and -5 eV) are mostly composed of a mixture of O-2p and Nb-4d orbitals. This suggests a partial covalent bond between Nb and O atoms. The conduction bands above the Fermi energy level are mostly composed of Nb-4p orbitals and Li-2s orbitals.

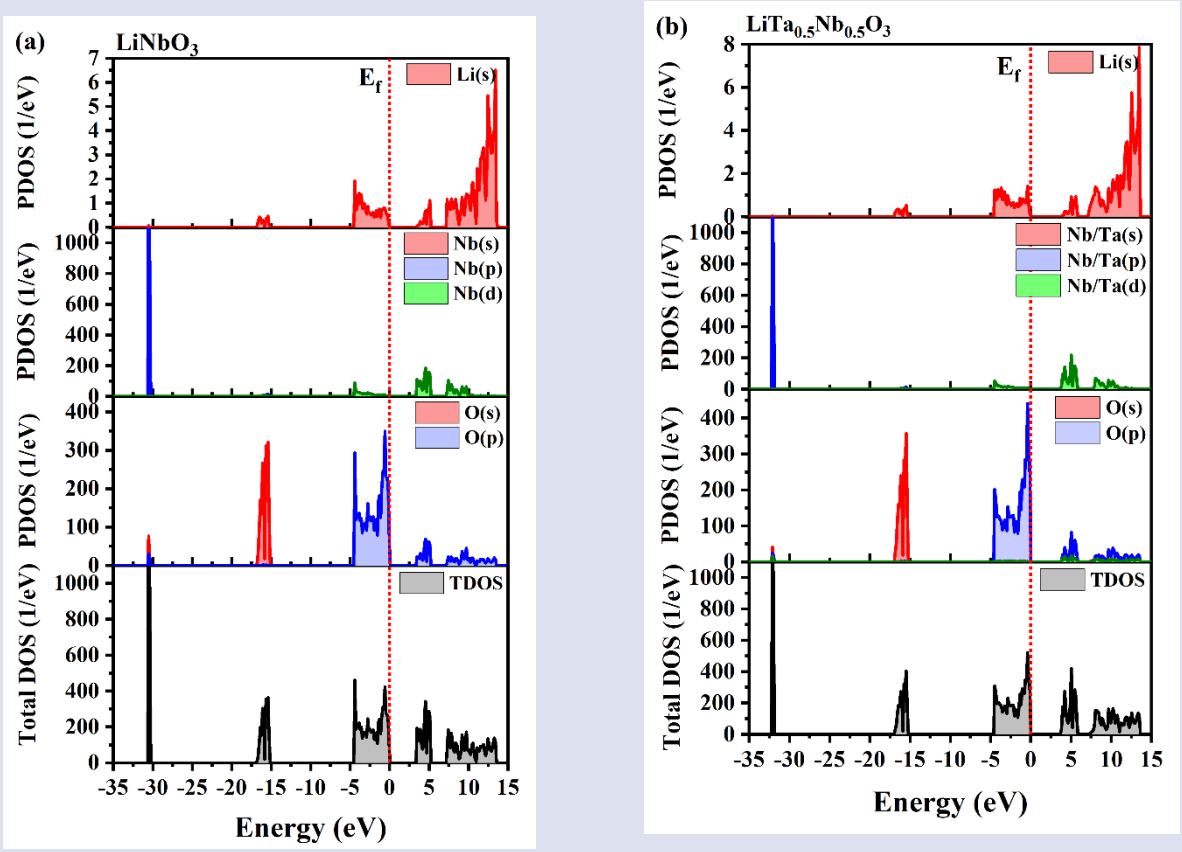

Figure 3. The partial (PDOS) and total density of states (TDOS) of $LiNb_{1-x}Ta_xO_3$ for (a) x= 0.0 and (b) x=0.5.

The electronic band structure and DOS were calculated for $LiNb_{1-x}Ta_xO_3$ by doping Ta at a rate of 0.1 from x=0.0 to x=1.0. However, the electronic band structure plots of $LiNb_{1-x}Ta_xO_3$ calculated for x=0 and x=0.5 are presented in Figure 2(a) and (b). As illustrated in Figure 2(a) and (b), the electronic band structure plots obtained by doping at x=0 and x=0.5 exhibit notable similarities. The band gap of $LiNb_{1-x}Ta_xO_3$ with 50% Ta doping was determined to be 3.79 eV. On the other hand, a closer examination of the DOS plots reveals that the Nb/Ta-4p orbitals exhibit a shift towards lower energies when Ta is introduced in place of Nb. The variation of the forbidden band gap for $LiNb_{1-x}Ta_xO_3$ from x=0.0 to x=1.0 with 0.1 Ta doping is given in Figure 4. As illustrated in Figure 4, the band gap of $LiNb_{1-x}Ta_xO_3$ exhibits an increase with Ta doping.

Optical Properties

Due to the symmetry of the $LiNbO_3$ crystal, the dielectric tensor has components only in the x- and z-directions. The real ($\varepsilon_1(\omega)$) and imaginary parts ($\varepsilon_2(\omega)$) of the calculated frequency-dependent complex dielectric function in the x- and z-axes for $LiNbO_3$ in the rhombohedral structure are given in Figures 5(a) and (b), respectively. The $\varepsilon_1(\omega)$ is related to the electronic polarizations of the materials. The $\varepsilon_2(\omega)$ determines the transition probability of electrons from occupied to unoccupied energy levels and is therefore related to optical absorption. The value of the $\varepsilon_1(\omega)$ in the zero frequency limit ($\varepsilon_1(0)$) is known as the static dielectric constant. As illustrated in Figure 5 (a) and (b), the values of the static dielectric constant were found to be 5.71 and 5.29 for the x- and z-directions, respectively. Aliabad [16] and et al. found 5.91 and 5.63 for x- and z-directions with GGA, respectively. Mamoun et al. [25] found 5.42 and 5.27 for x- and z-directions with GGA, respectively. It can be observed that the values obtained for the static dielectric constant are aligned with those reported in the existing literature.

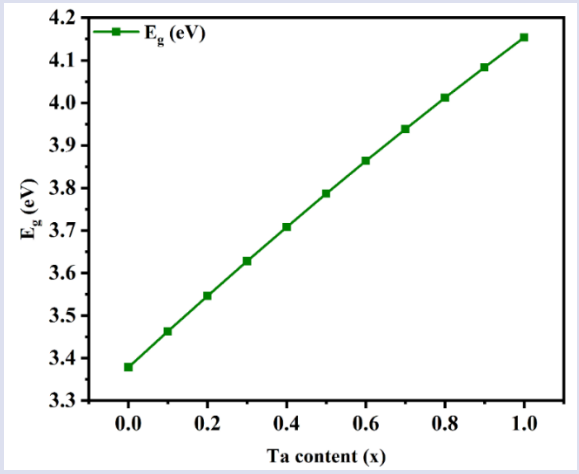

Figure 4. The calculated band gap as a function of Ta doping for $LiNb_{1-x}Ta_xO_3$

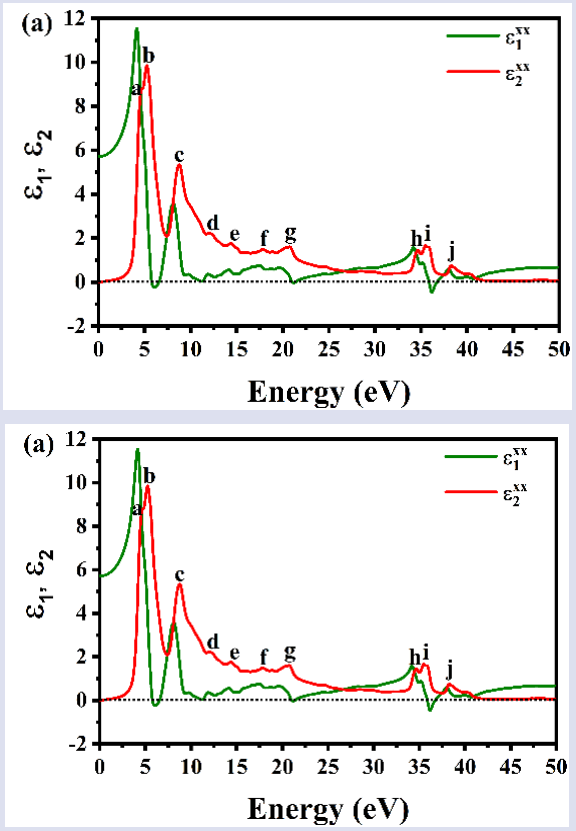

Figure 5. The real and imaginary parts of the dielectric function for $LiNbO_3$ along (a) x and (b) z-directions.

$\varepsilon_1(\omega)$ has negative values in the energy ranges of 5.42-6.09, 20.68-20.91 and 35.48-36.33 eV in the x-direction. The negative ranges of $\varepsilon_1(\omega)$ in the z-direction are in the energy ranges of 9.80-10.30, 20.53-21.62 and 35.41-36.44 eV, respectively. In these energy ranges where $\varepsilon_1(\omega)$ has negative values, the material shows metallic properties. As illustrated in Figure 5 (a) and (b), the first critical points of the $\varepsilon_2(\omega)$ occur around 2.4 eV in both x- and z-direction. These points correspond to the points where the valence band separates from the conduction band and are known as the fundamental absorption edge. After this point, the curves show a rapid increase as the number of points contributing to the $\varepsilon_2(\omega)$ increases abruptly. The $\varepsilon_2(\omega)$ exhibits a pronounced absorption peak at an energy value of 4.6 eV in both the x-direction and z-direction. These energy values correspond to optical transitions from O-2p states to Nb-4d states at Γ. The energy values corresponding to the other maximum peaks of $\varepsilon_2(\omega)$ are given in Table 3 together with the existing theoretical and experimental results. These values correspond to interband transitions at different higher symmetry points. Furthermore, as can be seen from Table 3, the results obtained are consistent with the findings of both theoretical and experimental studies reported in the existing literature.

Table 3. The energy values corresponding to the maximum peaks of $\varepsilon_2(\omega)$ for $LiNbO_3$ crystal.

	ε_2	a	b	c	d	e	f	g	h	i	j
x	GGA(Cal.)	4.6	5.2	8.7	11.9	14.3	17.8	20.8	34.6	35.5	38.3
	GGA[16]	4.2	4.98	8.75							
	GGA[25]	4.39	5.02	8.61							
	LDA[5]	4.97	5.21	8.87							
z	GGA(Cal.)	4.6	5.4	8.6	11.6	14.2	17.1	20.8	34.5	35.4	38.2
	GGA[16]	4.2	5.03	8.75							
	GGA[25]	4.37	5.24	8.67							
	LDA[5]	4.98	5.21	8.84							
	Exp.[26]	4.38	5.07	8.14	12.85	14.6	18.23	20.5			

The plots of the real parts of the dielectric function for $LiNb_{1-x}Ta_xO_3$ by increasing the Ta doping by 0.1 from x=0 to x=1 are given in Figures 6(a) and (b) for x- and z-directions, respectively. As can be seen from Figures 6(a) and (b), both the energy values corresponding to the maximum peaks of the $\varepsilon_1(\omega)$ and the negative energy values shift to higher energies with Ta doping. In contrast, the variation of the $\varepsilon_2(\omega)$ for $LiNb_{1-x}Ta_xO_3$ with Ta doping is given in Figures 6(c) and (d). Since Nb and Ta atoms have similar electronic configuration, there is not much difference in the variation of the $\varepsilon_2(\omega)$ for $LiNb_{1-x}Ta_xO_3$ with Ta doping. Only with Ta doping, the absorption edges and the maximum peaks shift to higher energies. This suggests that the BO_6 octahedron plays a significant role in establishing the upper edge of the valence band and the edge of the conduction band in ABO_3-type perovskite structures. The results obtained are consistent with those presented in Figure 4.

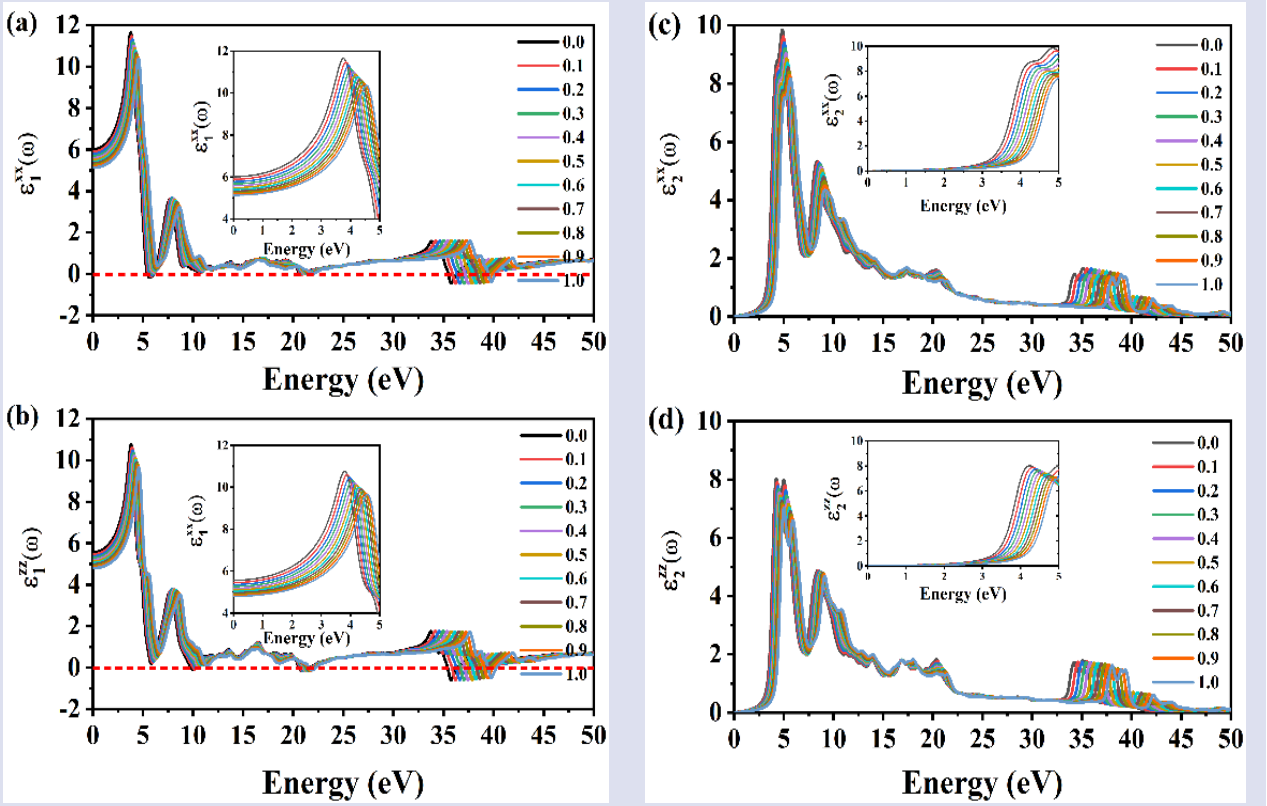

Figure 6. The real and imaginary parts of the dielectric function as a function of Ta doping for $LiNb_{1-x}Ta_xO_3$.

Mechanical Properties

One of the most essential properties of solids is their elastic constants. An understanding of the elastic constants of solids establishes a connection between the mechanical and dynamic behavior of crystals, and provides valuable insight into the nature of the forces that act within solids. The propagation of an elastic wave in a medium is closely related to the elastic constants of that material. Furthermore, elastic constants are associated with thermodynamic properties, including Debye temperature, coefficient of thermal expansion, melting point, and specific heat. The elastic constants provide insight into the response of a solid material to externally applied forces. The mechanical properties of solids can be ascertained through the utilization of elastic constants. In particular, they provide information regarding the physical properties of materials, including mechanical stability, stiffness, ductility, and brittleness. The elastic moduli, including the bulk modulus (B), shear modulus (G), Young's modulus (E), and Poisson's ratio (ν), are derived from single-crystal elastic constants [17]. Due to the symmetry of the $LiNbO_3$ crystal, it has eight components $C_{11}, C_{12}, C_{13}, C_{14}, C_{33}, C_{44}, C_{65}$ and C_{66} in the rhombohedral structure. Since $C_{65} = C_{14}$ and $C_{66} = 1/2\,(C_{11} - C_{12})$, the number of independent components is six. For a mechanically stable rhombohedral structure, it is necessary that the elastic constants provide the Born stability criteria, which are as follows [27]:

$$(C_{11} - C_{12}) > 0, \quad (C_{11} + C_{12}) > 0, \quad C_{33} > 0,$$
$$C_{44} > 0 \quad (C_{11} + C_{12})C_{33} - 2C_{13}^2 > 0, \quad (1)$$
$$(C_{11} + C_{12})C_{33} - 2C_{13}^2 > 0, \quad (C_{11} - C_{12})C_{44} - 2C_{14}^2 > 0$$

The calculated elastic constants for the $LiNbO_3$ crystal are presented in Table 4. As shown in Table 4, the calculated elastic constants for the $LiNbO_3$ crystal fulfill the Born stability criteria required for the rhombohedral structure. The elastic constants C_{11} and C_{33} indicate the resistance to linear compression along the x- and z- axes of the crystal, while the elastic constants $C_{12}, C_{13}, C_{14}, C_{44}$ and C_{66} are related to the elasticity in the shape of the crystal. Since $C_{33} > C_{11}$, the z-direction demonstrates more resistance to unidirectional deformation than the x-direction. It is also seen from Table 4 that the calculated results for $LiNbO_3$ crystal are close to the theoretical and experimental results available in the literature.

Table 4. The elastic constants (GPa) of LiNbO3 in the rhombohedral structure.

Ref.	C_{11}	C_{12}	C_{13}	C_{14}	C_{33}	C_{44}	C_{66}
GGA(Cal.)	184.5	58.9	60.5	17.5	220.1	39.7	62.7
Exp.[28]	198.39	54.72	65.13	7.88	227.9	59.65	
Exp.[29]	198.86	54.67	67.99	7.83	234.18	59.85	72.09
Exp.[30]	198.86	54.67	67.26	7.83	233.7	59.85	
Exp.[31]	198.9	54.7	67.3	7.8	233.7	70.4	72.1
Exp.[32] (Smp-1)	199.2	54.7	70	7.9	240	59.9	72.2
Exp.[32] (Smp-2)	198.6	54.7	69	7.8	238	59.8	71.9
Exp.[32] (Smp-3)	199.9	55.6	70	7.8	240	60	72.2
GGA[33]	208.77	73.28	75.99	15.68	236.23	49.80	67.74
LDA[17]	205.69	69.28	72.15	12.38	238.34	65.81	70.03

The variation of the second-order elastic constants for $LiNb_{1-x}Ta_xO_3$ with Ta doping is given in Figure 7(a). As can be seen from Figure 7(a), the elastic constants C_{11} and C_{33} increase linearly with Ta doping. The doping of Ta makes the $LiNbO_3$ compound more resistant to unidirectional compression along the main crystallographic axes. In contrast, as can be seen from Figure 7(a), C_{66} increases slightly with the doping of Ta, but C_{13} does not change very much with the doping of Ta. On the other hand, the C_{12} and C_{14} values of the $LiNb_{1-x}Ta_xO_3$ decrease with the doping of Ta. This means that $LiNb_{1-x}Ta_xO_3$ becomes less resistant to lateral deformation. As illustrated in Figure 7(a), the elastic constant C_{44} shows the most different response to Ta doping. The C_{44} shows a rapid increase up to 50% Ta doping and does not change much after 50% Ta doping.

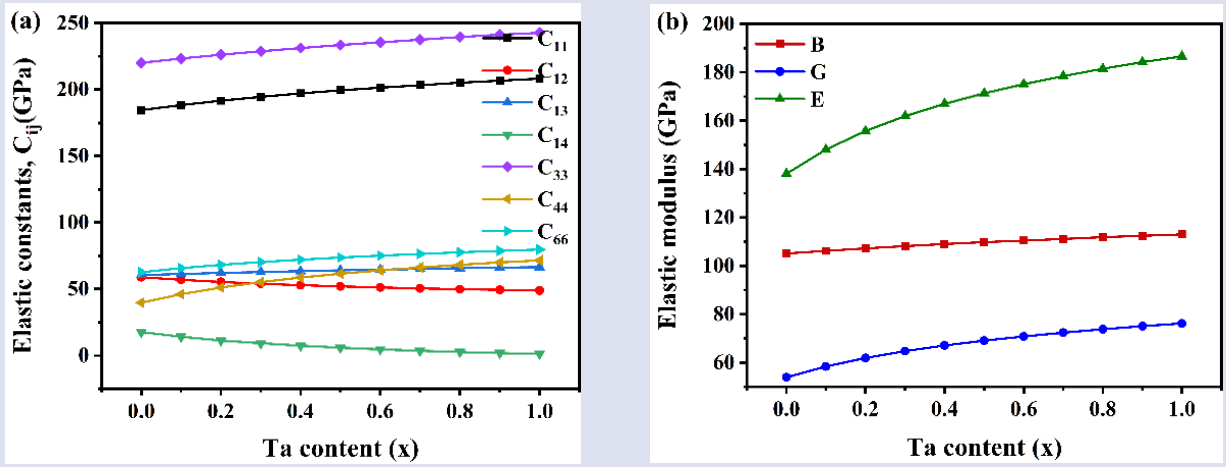

Figure 7. The calculated elastic constants (a) and elastic modulus (b) as a function of Ta doping for $LiNb_{1-x}Ta_xO_3$..

The mechanical properties of polycrystalline materials can be determined from the single crystal elastic constants using two basic methods, known as the Voigt [34] and Reuss [35] method. In the Voigt method (B_V and G_V) and the Reuss method (B_R and G_R), the bulk and shear moduli are given by the following equations:

$$B_V = \frac{1}{9}[2(C_{11} + C_{12} + 2C_{13}) + C_{33}] \quad (2)$$

$$G_V = \frac{1}{30}[C_{11} + C_{12} + 2(C_{33} - 2C_{13}) + 12(C_{44} + C_{66})] \quad (3)$$

$$B_R = \frac{(C_{11} + C_{12})C_{33} - 2C_{13}^2}{C_{11} + C_{12} + 2C_{33} - 4C_{13}} \quad (4)$$

$$G_R = \frac{2}{5}\frac{[(C_{11} + C_{12})C_{33} - 2C_{13}^2]C_{44}C_{66}}{3B_VC_{44}C_{66} + [(C_{11} + C_{12})C_{33} - 2C_{13}^2](C_{44} + C_{66})} \quad (5)$$

Using Voigt-Reuss-Hill approximations [36], the bulk and shear moduli are given as follows:

$$B = \frac{1}{2}(B_V + B_R) \quad (6)$$

$$B = \frac{1}{2}(G_V + G_R) \quad (7)$$

E and ν are elastic parameters that are often used to investigate the stiffness of solids, which can be calculated using B and G with the following equations [17].

$$E = \frac{9BG}{3B + G} \quad (8)$$

$$\nu = \frac{3B - 2G}{2(3B + G)} \quad (9)$$

The values of B, G, E and υ of $LiNbO_3$ calculated in the rhombohedral structure are given in Table 5. As shown in Table 5, the values of B and G found in this study are close to the values found by Tripathy et al. [33]. However, the values of B and G found by Hossain [17] are larger than our values.

Table 5. The bulk modulus B (GPa), shear modulus G (GPa), Young's modulus E (GPa) and Poisson's ratio (υ) of $LiNbO_3$ in the rhombohedral structure.

Referans	B_V	B_R	B	G_V	G_R	G	E	B/G	υ
GGA[Cal.]	105.4	104.7	105.1	55.7	52.1	53.9	138.1	1.95	0.281
LDA[17]			272.80			138.77	355.95	1.97	0.28
GGA[33]			122.25			62.03			

The variation of B, G and E values calculated for $LiNb_{1-x}Ta_xO_3$ with Ta doping is given in Figure 7(b). As can be seen from Figure 7(b), B increases linearly with Ta doping. This shows that $LiNb_{1-x}Ta_xO_3$ is more resistant to compression under hydrostatic pressure with Ta doping. On the other hand, as can be seen from Figure 7(b), the values of G, which expresses the resistance to plastic deformation, and E, which defines a measure of the hardness of the material, exhibit a more pronounced increase with Ta doping.

Table 6. The bulk modulus (B_V and B_R), shear modulus (G_V and G_R), Poisson's ratio (υ) and B/G ratio as a function of Ta doping for $LiNb_{1-x}Ta_xO_3$.

Content (x)	B_V	B_R	G_V	G_R	υ	B/G
0.0	105.4	104.7	55.7	52.1	0.281	1.950
0.1	106.5	105.8	59.6	57.2	0.267	1.817
0.2	107.6	106.8	62.8	61.1	0.258	1.731
0.3	108.6	107.6	65.4	64.1	0.250	1.670
0.4	109.5	108.5	67.6	66.6	0.245	1.625
0.5	110.3	109.3	69.5	68.7	0.240	1.589
0.6	111.0	109.9	71.1	70.5	0.236	1.560
0.7	111.7	110.6	72.7	72.1	0.232	1.536
0.8	112.5	111.3	74.0	73.6	0.230	1.516
0.9	113.1	111.9	75.3	74.9	0.227	1.498
1.0	113.7	112.4	76.4	76.0	0.225	1.484

The Poisson's ratio υ provides valuable insight into the nature of interatomic bonds in solids. The value of Poisson's ratio for covalent materials is υ~0.1, for ionic materials υ=0.25 and for metallic materials υ=0.33 [37]. Table 6 shows the value of υ with Ta doping. As shown in Table 6, the ionic contribution is dominant in the interatomic bond for $LiNb_{1-x}Ta_xO_3$.

As Pugh [38] has previously established, the B/G ratio can be employed to ascertain whether a given material exhibits brittle (B/G < 1.75) or ductile (B/G > 1.75) behavior. As can be seen from Table 6, $LiNb_{1-x}Ta_xO_3$ exhibits a transition from a ductile to a more brittle state with increasing Ta doping.

The macro (H_{mac}) and micro (H_{mic}) hardness of materials can be determined by a theoretical model, as described in [39],

$$H_{macro} = 2\left(\frac{G^3}{B^2}\right)^{0.585} - 3 \qquad (10)$$

$$H_{micro} = \frac{(1-2\nu)Y}{6(1+\nu)} \qquad (11)$$

The obtained H_{mac} and H_{mic} hardness values of $LiNbO_3$ are 6.43 GPa and 7.87 GPa, respectively. According to the definition, a material is considered soft if its Vickers hardness is less than 10 GPa [40], while a material is classified as super hard if its Vickers hardness is greater than 40 GPa [37]. According to our calculation, the $LiNbO_3$ can be classified as a soft material due to its Vickers hardness values lower than 10 GPa. As seen from Figure 8, the H_{mac} and H_{mic} hardness values of $LiNb_{1-x}Ta_xO_3$ increase with Ta doping, and it can be classified as a medium hard material after approximately 40% Ta doping.

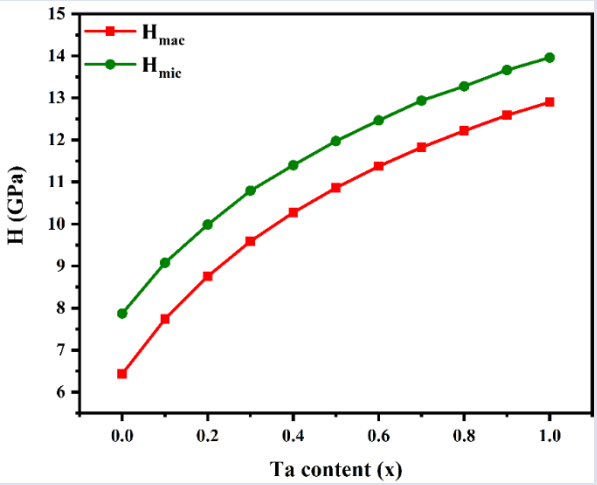

Figure 8. The calculated macro (H_{mac}) and micro (H_{mic}) hardnes of $LiNb_{1-x}Ta_xO_3$ as a function of Ta doping.

Conclusion

In conclusion, the structural, electronic, optical and mechanical properties of pure and Ta doped $LiNbO_3$ in the ferroelectric phase have been obtained by using the DFT with the GGA. It was demonstrated that pure $LiNbO_3$ is a direct bandgap material, exhibiting a forbidden energy gap of 3.38 eV at the Γ point in the Brillouin zone. The calculation results indicated that the lattice parameter of $LiNb_{1-x}Ta_xO_3$ decreases with Ta doping, but the forbidden energy gap increases. The frequency-dependent complex dielectric functions of pure and Ta doped $LiNbO_3$ are calculated. Both the energy values corresponding to the maximum peaks of the real parts of the dielectric function and the negative energy values shift to higher energies with Ta doping. The results show that the absorption edges of $LiNb_{1-x}Ta_xO_3$ shift to higher energies with Ta doping. The calculated elastic constants indicated that pure and Ta doped $LiNbO_3$ are mechanically stable. Through the calculated υ and B/G values, it is concluded that the rhombohedral structure of $LiNbO_3$ is ionic and ductile, but with increasing Ta doping, it exhibits a transition from ductile to a more brittle state. Finally, from the calculated H_{mac} and H_{mic} hardness values, it was determined that pure $LiNbO_3$ is a soft material, but after 40% Ta doping, it exhibits a transition to a medium hard material.

Conflict of interest

There are no conflicts of interest in this work.

Acknowledgment

This study was supported by Research Fund of the Hakkari University. Project Number: FM21LTP1

References

[1] Bridges F., Castillo-Torres J., Car B., Medling S., Kozina M., EXAFS evidence for a primary Zn Li dopant in $LiNbO_3$, *Physical Review B—Condensed Matter and Materials Physics*, 85 (2012) 064107-064118.

[2] He Y.L., Xue D.F., Bond-energy study of photorefractive properties of doped lithium niobate crystals, *J Phys Chem C*, 111 (2007) 13238-13243.

[3] Tsuboi T., Grinberg M., Kaczmarek S.M., Site symmetries of Cu^{2+} ions in LiNbO3 crystals, *J Alloy Compd*, 341 (2002) 333-337.

[4] Wang W., Wang R., Zhang W., Xing L.L., Xu Y.L., Wu X.H., A computer study and photoelectric property analysis of potassium-doped lithium niobate single crystals, *Phys Chem Chem Phys*, 15 (2013) 14347-14356.

[5] Cabuk S., First-Principles Study of The Electronic, Linear, and Nonlinear Optical Properties of Li(Nb, Ta)O_3, *Int J Mod Phys B*, 24 (2010) 6277-6290.

[6] Ok K.M., Chi E.O., Halasyamani P.S., Bulk characterization methods for non-centrosymmetric materials: second-harmonic generation, piezoelectricity, pyroelectricity, and ferroelectricity, *Chem Soc Rev*, 35 (2006) 710-717.

[7] Xu Y.H., Hao X.F., Franchini C., Gao F.M., Structural, Electronic, and Ferroelectric Properties of Compressed $CdPbO_3$ Polymorphs, *Inorg Chem*, 52 (2013) 1032-1039.

[8] Yu C.J., Emmerich H., An efficient virtual crystal approximation that can be used to treat heterovalent atoms, applied to (1−x)$BiScO_3$–x$PbTiO_3$, *J Phys-Condens Mat*, 19 (2007).

[9] Perdew J.P., Burke K., Ernzerhof M., Generalized gradient approximation made simple, *Phys Rev Lett*, 77 (1996) 3865-3868.

[10] Hamann D.R., Optimized norm-conserving Vanderbilt pseudopotentials, *Phys Rev B*, 88 (2013).

[11] Monkhorst H.J., Pack J.D., Special points for Brillouin-zone integrations, *Phys Rev B*, 13 (1976) 5188.

[12] Gonze X., Amadon B., Antonius G., Arnardi F., Baguet L., Beuken J.M., Bieder J., Bottin F., Bouchet J., Bousquet E., Brouwer N., Bruneval F., Brunin G., Cavignac T., Charraud J.B., Chen W., Côté M., Cottenier S., Denier J., Geneste G., Ghosez P., Giantomassi M., Gillet Y., Gingras O., Hamann D.R., Hautier G., He X., Helbig N., Holzwarth N., Jia Y.C., Jollet F., Lafargue-Dit-Hauret W., Lejaeghere K., Marques M.A.L., Martin A., Martins C., Miranda H.P.C., Naccarato F., Persson K., Petretto G., Planes V., Pouillon Y., Prokhorenko S., Ricci F., Rignanese G.M., Romero A.H., Schmitt M.M., Torrent M., van Setten M.J., Van Troeye B., Verstraete M.J., Zerah G., Zwanziger J.W., The ABINIT project: Impact, environment and recent developments, *Comput Phys Commun*, 248 (2020) 107042.

[13] Megaw H.D., A note on the structure of lithium niobate, $LiNbO_3$, *Acta Crystallographica Section A: Crystal Physics, Diffraction, Theoretical and General Crystallography*, 24 (1968) 583-588.

[14] Bermúdez V., Aragó C., Fernández-Ruiz R., Diéguez E., Evolution of the Structural Properties in Ferroelectric $LiNb_{1-x}Ta_xO_3$ Compound with Variation in Ta Composition, *Ferroelectrics*, 304 (2004) 989-992.

[15] Schmidt W.G., Albrecht M., Wippermann S., Blankenburg S., Rauls E., Fuchs F., Rödl C., Furthmüller J., Hermann A., $LiNbO_3$ ground- and excited-state properties from first-principles calculations, *Phys Rev B*, 77 (2008).

[16] Aliabad H.A.R., Ahmad I., Optoelectronic properties of $Li_xA_xNbO_3$ (A: Na, K, Rb, Cs, Fr) crystals, *Physica B*, 407 (2012) 368-377.

[17] Hossain M.M., First principles study on the structural, elastic, electronic and optical properties of $LiNbO_3$, *Heliyon*, 5 (2019).

[18] Dhar A., Mansingh A., Optical properties of reduced lithium niobate single crystals, *J Appl Phys*, 68 (1990) 5804-5809.

[19] Javid M.A., Khan Z.U., Mehmood Z., Nabi A., Hussain F., Imran M., Nadeem M., Anjum N., Structural, electronic and optical properties of $LiNbO_3$ using GGA-PBE and TB-mBJ functionals: A DFT study, *Int J Mod Phys B*, 32 (2018).

[20] Xu Y.-N., Gu Z.-Q., Ching W., Calculation of self-energy corrected band structure of rhombohedral $LiNbO_3$, *Ferroelectrics*, 164 (1995) 225-230.

[21] Thierfelder C., Sanna S., Schindlmayr A., Schmidt W.G., Do we know the band gap of lithium niobate?, *Phys Status Solidi C*, 7 (2010) 362-365.

[22] Nahm H.H., Park C.H., First-principles study of microscopic properties of the Nb antisite in $LiNbO_3$: Comparison to phenomenological polaron theory, *Phys Rev B*, 78 (2008).

[23] Kato H., Kudo A., Water splitting into H_2 and O_2 on alkali tantalate photocatalysts $ATaO_3$ (A= Li, Na, and K), *The Journal of Physical Chemistry B*, 105 (2001) 4285-4292.

[24] Wang H., Wu F., Jiang H., Electronic band structures of $ATaO_3$ (A= Li, Na, and K) from first-principles many-body perturbation theory, *The Journal of Physical Chemistry C*, 115 (2011) 16180-16186.

[25] Mamoun S., Merad A.E., Guilbert L., Energy band gap and optical properties of lithium niobate from ab initio calculations, *Comp Mater Sci*, 79 (2013) 125-131.

[26] Mamedov A.M., Osman M.A., Hajieva L.C., VUV Reflectivity of $LiNbO_3$ and $LiTaO_3$ Single Crystals, *Appl. Phys. A*, 34 (1984) 189-192.

[27] Wang J.J., Meng F.Y., Ma X.Q., Xu M.X., Chen L.Q., Lattice, elastic, polarization, and electrostrictive properties of BaTiO3 from first-principles, *J Appl Phys*, 108 (2010).

[28] Kovacs G., Anhorn M., Engan H.E., Visintini G., Ruppel C.C.W., Improved Material Constants for $LiNbO_3$ and $LiTaO_3$, *IEEE Ultrasonics Symposium*, 438 (1990) 1-4.

[29] Kushibiki J.I., Takanaga I., Arakawa M., Sannomiya T., Accurate Measurements of the Acoustical Physical Constants of $LiNbO_3$ and $LiTaO_3$ Single Crystals, IEEE Transactions on ultrasonics, ferroelectrics, and frequency control, 1999, 1315-1323

[30] Takanaga I., Kushibiki J.I., A Method of Determining Acoustical Physical Constants for Piezoelectric Materials by Line-Focus-Beam Acoustic Microscopy, IEEE Transactions on ultrasonics, ferroelectrics, and frequency control, 2002, 893-904

[31] Philip T., Menon C.S., Induleka K., Higher Order Elastic Constants, Gruneisen Parameters and Lattice Thermal Expansion of Lithium Niobate, *E-Journal of Chemistry*, 3 (2006) 122-133.

[32] Andrushchak A.S., Mytsyk B.G., Laba H.P., Yurkevych O.V., Solskii I.M., Kityk A.V., Sahraoui B., Complete sets of elastic constants and photoelastic coefficients of pure and MgO-doped lithium niobate crystals at room temperature, *J Appl Phys*, 106 (2009).

[33] Tripathy S.K., Sahu G., Ground state properties of $LiNbO_3$ from first-principles calculations, Advanced Materials and Radiation Physics (AMRP-2015): 4th National Conference on Advanced Materials and Radiation Physics, Longowal, India, 2015, 020005

[34] Voigt W., Lehrbuch der Kristallphysik Teubner Verlag, Leipzig1910.

[35] Reuss A., Berechung der Fliessgrenze von Mischkristallen, *Z. Angew. Math. Mech*, 9 (1929).

[36] Hill R., The elastic behaviour of a crystalline aggregate, *Proceedings of the Physical Society. Section A*, 65 (1952) 349.

[37] Haines J., Léger J.M., Bocquillon G., Synthesis and design of superhard materials, *Ann Rev Mater Res*, 31 (2001) 1-23.

[38] Pugh S., XCII. Relations between the elastic moduli and the plastic properties of polycrystalline pure metals, *The London, Edinburgh, and Dublin Philosophical Magazine and Journal of Science*, 45 (1954) 823-843.

[39] Ali M.A., Hossain M.M., Islam A.K.M.A., Naqib S.H., Ternary boride Hf_3PB_4: Insights into the physical properties of the hardest possible boride MAX phase, *J Alloy Compd*, 857 (2021) 158264.

[40] Liu W.N., Niu Y.T., Li W.Q., Theoretical prediction of the physical characteristic of Na_3MO_4 (M = Np and Pu): The first-principles calculations, *Ceram Int*, 46 (2020) 25359-25365.